Prepared for submission to JCAP

Local real space operators for translating Q/U to E/B

Abstract. We derive real space Q/U to E/B operators on the sphere and demonstrate their numerical equivalence to the harmonic space methods. In process we also derive real space operators which allow direct decomposition of measured Q/U into those corresponding to E-modes and B-modes respectively. These operators are derived on the sphere and they duly account for the curvature effects. These analytical derivations reveal a function form for the radial kernel, allowing us to quantify the non-local nature of the E and B fields and their dependence on the band limit of the measurement. These estimators suggest the possibility of constructing more locally defined E and B maps, by making a suitable choice for the radial filter. Such local E and B maps may help partially mitigate the foreground leakage issue across the two modes. Since these operators allow the computation of E and B field in each pixel by integrating in a small region around the pixel, these operation can easily parallelized. We note that due to the local nature of these operators, it is challenging to reliably measure modes on large angular scales $\ell < 50$.

Contents

1 Introduction

In this work we follow the convection in which bar-ed variables correspond to those in real space, while the tilde-ed variables correspond to those in harmonic space.

2 E/B description of CMB polarization

2.1 Polarization primer

The CMB polarization is measured in terms of the Stokes Q and U parameters. These measurements can be combined to form the complex spin 2 polarization field as follows,

$$ {}_{\pm2}X(\hat{n}) = Q(\hat{n}) \pm iU(\hat{n}) = \sum_{\ell m} {}_{\pm2}X_{\ell m}\, {}_{\pm2}Y_{\ell m}(\hat{n}) $$

Since these measured quantities depend on the local coordinate system, it is cumbersome to work with them. To overcome this, one often describes the CMB polarization field in terms of two scalar fields denoted by $E(\hat{n})$ and $B(\hat{n})$, which are related to ${}_{\pm2}X(\hat{n})$ through the following expression,

$$ E(\hat{n}) = -\frac{1}{2}\left[\bar{\eth}^2_{+2}X(\hat{n}) + \eth^2_{-2}X(\hat{n})\right] \;;\; B(\hat{n}) = -\frac{1}{2i}\left[\bar{\eth}^2_{+2}X(\hat{n}) - \eth^2_{-2}X(\hat{n})\right], \tag{2.1} $$

where $\eth$ and $\bar{\eth}$ denote the spin raising and lowering operators respectively. E and B fields are spin-0 fields similar to the temperature anisotropies and hence their value are independent of the coordinate system definitions. The spin raising and lowering operators are known to have the following properties,

$$ \eth_s Y_{lm}(\hat{n}) = \sqrt{(\ell - s)(\ell + s + 1)}\, {}_{s+1}Y_{lm}(\hat{n}), \tag{2.2a} $$

$$ \bar{\eth}_s Y_{lm}(\hat{n}) = -\sqrt{(\ell + s)(\ell - s + 1)}\, {}_{s-1}Y_{lm}(\hat{n}), \tag{2.2b} $$

where ${}_sY_{lm}(\hat{n})$ are the spin spherical harmonics.

Using Eq. (2.1) and the properties of the spin raising and lowering operators given in Eq. (2.2a) it can be shown that the E/B fields are given by the following set of equations,

$$ E(\hat{n}) = \sum_{\ell m} e_{\ell m}\sqrt{\frac{(\ell+2)!}{(\ell-2)!}}Y_{\ell m}(\hat{n}) \;;\; B(\hat{n}) = \sum_{\ell m} b_{\ell m}\sqrt{\frac{(\ell+2)!}{(\ell-2)!}}Y_{\ell m}(\hat{n}), \tag{2.3} $$

where the harmonic coefficients of the E/B fields are related to the spin harmonic coefficients of the polarization field through the following equations,

$$ e_{\ell m} = -\frac{1}{2}\left[{}_+X_{\ell m} +_- X_{\ell m}\right] \;;\; b_{\ell m} = -\frac{1}{2i}\left[{}_+X_{\ell m} -_- X_{\ell m}\right] \tag{2.4} $$

In the remainder of this article, the E/B modes will refer to those defined without the factor $\sqrt{\frac{(\ell+2)!}{(\ell-2)!}}$ seen in Eq. (2.3)

2.2 Matrix notation

Note that from this section onwards, we denote real space quantities using bar-ed variable while the harmonic space quantities are denoted by tilde-ed variables. Here we cast the relation introduced in Sec. 2.1 in matrix notation. This representation will make transparent the derivation of the real space operators we discuss in the following sections. We begin by introducing the matrices encoding the basis vectors,

$$ {}_sB = \begin{bmatrix} {}_{+s}Y & 0 \\ 0 & {}_{-s}Y \end{bmatrix}_{2\mathrm{N_{pix}} \times 2\mathrm{N_{alms}}} , \tag{2.5} $$

where s denotes the spin and we will only be working with cases $s \in 0, 2$. Note that this matrix is in general not a square matrix. Its shape is determined by the data discretization scheme and the band limit of the data being studied.

Next we write down the different data vectors and their representation in real and harmonic space,

$$ \bar{S} = \begin{bmatrix} E \\ B \end{bmatrix}_{2\mathrm{N_{pix}} \times 1} \quad ; \quad \bar{X} = \begin{bmatrix} {}_{+2}X \\ {}_{-2}X \end{bmatrix}_{2\mathrm{N_{pix}} \times 1} \quad ; \quad \bar{P} = \begin{bmatrix} Q \\ U \end{bmatrix}_{2\mathrm{N_{pix}} \times 1} , \tag{2.6a} $$

$$ \tilde{S} = \begin{bmatrix} a^E \\ a^B \end{bmatrix}_{2\mathrm{N_{alms}} \times 1} \quad ; \quad \tilde{X} = \begin{bmatrix} {}_{+2}\tilde{X} \\ {}_{-2}\tilde{X} \end{bmatrix}_{2\mathrm{N_{alms}} \times 1} , \tag{2.6b} $$

and the matrix operators which govern the transformations between them,

$$ \bar{T} = \begin{bmatrix} \mathbb{1} & i\mathbb{1} \\ \mathbb{1} & -i\mathbb{1} \end{bmatrix}_{2\mathrm{N_{pix}} \times 2\mathrm{N_{pix}}} \quad ; \quad \bar{T}^{-1} = \frac{1}{2}\bar{T}^\dagger , \tag{2.7a} $$

$$ \tilde{T} = -\begin{bmatrix} \mathbb{1} & i\mathbb{1} \\ \mathbb{1} & -i\mathbb{1} \end{bmatrix}_{2\mathrm{N_{alms}} \times 2\mathrm{N_{alms}}} \quad ; \quad \tilde{T}^{-1} = \frac{1}{2}\tilde{T}^\dagger . \tag{2.7b} $$

The different data vectors are related via the following relations,

$$ \tilde{X} = {}_2B^\dagger * \bar{X} , \tag{2.8a} $$

$$ \bar{X} = \bar{T} * \bar{P} \quad ; \quad \tilde{X} = \tilde{T} * \tilde{S} , \tag{2.8b} $$

$$ \bar{P} = \frac{1}{2}\bar{T}^\dagger * \bar{X} \quad ; \quad \tilde{S} = \frac{1}{2}\tilde{T}^\dagger * \tilde{X} . \tag{2.8c} $$

$$ \bar{S} = {}_0B * \tilde{S} \tag{2.8d} $$

Finally we introduce the harmonic space operators, which project the data vector to E or B subspace,

$$ \tilde{O}_E = \begin{bmatrix} \mathbb{1} & \mathbb{0} \\ \mathbb{0} & \mathbb{0} \end{bmatrix}_{2\mathrm{N_{alms}} \times 2\mathrm{N_{alms}}} \quad ; \quad \tilde{O}_B = \begin{bmatrix} \mathbb{0} & \mathbb{0} \\ \mathbb{0} & \mathbb{1} \end{bmatrix}_{2\mathrm{N_{alms}} \times 2\mathrm{N_{alms}}} , \tag{2.9a} $$

$$ \tilde{S}_E = \tilde{O}_E * \tilde{S} \quad ; \quad \tilde{S}_B = \tilde{O}_B * \tilde{S} . \tag{2.9b} $$

Note that these matrices are idempotent and are orthogonal to each other, indicated by the following relations,

$$ \tilde{O}_E * \tilde{O}_E = \tilde{O}_E \quad ; \quad \tilde{O}_B * \tilde{O}_B = \tilde{O}_B , \tag{2.10a} $$

$$ \tilde{O}_E * \tilde{O}_B = \mathbb{0} , \tag{2.10b} $$

$$ \tilde{O}_E + \tilde{O}_B = \mathbb{1} . \tag{2.10c} $$

Here it is important to note that these relations are exact in harmonic space. On the contrary, the operators in real space are are not exact owing to the band limit imposed by the finite resolution of the measurements.

3 Real space operators

In this section we derive the real space operators which translate the Stokes parameters Q & U to E & B fields and vice versa and also derive real space operators for directly(without first evaluating the E & B field themselves) decomposing the Stokes Q & U parameters to those corresponding to E & B fields respectively. We extensively use the matrix notation introduces in Sec. 2.2 to make these derivations.

All the results are expressed as functions of the Euler angles α, β & γ on the sphere, which define the rotational transformations between the local cartesian coordinate system defined at the sphere locations $\hat{n}_i$ and $\hat{n}_j$. The Euler angles can be evaluated as the following functions of the angular coordinates of the points $\hat{n}_i \equiv (\theta_i, \phi_i)$ and $\hat{n}_j \equiv (\theta_j, \phi_j)$,

$$\cos(\beta) = \sin(\theta_i)\sin(\theta_j)\cos(\phi_i - \phi_j) + \cos(\theta_i)\cos(\theta_j)\,, \tag{3.1a}$$

$$\tan(\alpha) = \frac{\sin(\phi_i - \phi_j)\sin(\theta_i)\sin(\theta_j)}{\cos(\theta_i)\cos(\beta) - \cos(\theta_j)}\,, \tag{3.1b}$$

$$\tan(\gamma) = \frac{\sin(\phi_i - \phi_j)\sin(\theta_i)\sin(\theta_j)}{\cos(\theta_j)\cos(\beta) - \cos(\theta_i)}\,. \tag{3.1c}$$

While evaluating these one needs to ensure that $\beta \in [0, \pi]$ and that $\alpha, \gamma \in [-\pi, \pi]$ are assigned the proper sign after duly accounting for the signs of the term in the numerator and the denominator in the expressions above. β denotes the angular distance between the two points on the sphere, while the angles α & γ define rotations which coalign the coordinate axes of the two coordinate systems.

3.1 Evaluating E & B fields from measured Stokes parameters Q & U

Using Eq. (2.8a), we can write down the relation between the real space vector of scalars and $\bar{S}^\dagger = [E, B]$ the polarization vector $\bar{P}^\dagger = [Q, U]$ as,

$$\bar{S} = {}_0B * \tilde{T}^{-1} * {}_2B^\dagger * \bar{T} * \bar{P} = \frac{1}{2}{}_0B * \tilde{T}^\dagger {}_2B^\dagger * \bar{T} * \bar{P} \tag{3.2a}$$

$$= \bar{O} * \bar{P} \tag{3.2b}$$

On contracting over the matrix operators action on $\bar{P}$, it can be shown that the operations reduce to the following matrix,

$$\bar{O} = \begin{bmatrix} -\mathcal{M}_r & -\mathcal{M}_i \\ \mathcal{M}_i & -\mathcal{M}_r \end{bmatrix}_{2N_{\rm pix} \times 2N_{pix}} \tag{3.3}$$

where $\mathcal{M}_r$ & $\mathcal{M}_i$ are given by the following relations,

$$\mathcal{M}(\hat{n}_i, \hat{n}_j) = \sum_{\ell m} {}_0Y_{\ell m}(\hat{n}_i) {}_2Y^*_{\ell m}(\hat{n}_j) = \sum_\ell \sqrt{\frac{2\ell+1}{4\pi}}\, {}_0Y^*_{\ell 2}(\beta_{ij}, \alpha_{ij})\,. \tag{3.4a}$$

$$= \mathcal{M}_r + i\mathcal{M}_i\,,$$

$$\mathcal{M}_r + i\mathcal{M}_i = \Big[\cos(2\alpha_{ij}) - i\sin(2\alpha_{ij})\Big] \sum_\ell \frac{2\ell+1}{4\pi}\sqrt{\frac{(\ell-2)!}{(\ell+2)!}} P_{\ell 2}(\cos\beta_{ij})\,, \tag{3.4b}$$

Therefore the real space operator is explicitly given by the following expression,

$$\bar{O} = -f(\beta_{ij}) \begin{bmatrix} \cos(2\alpha_{ij}) & \sin(2\alpha_{ij}) \\ -\sin(2\alpha_{ij}) & \cos(2\alpha_{ij}) \end{bmatrix} , \tag{3.5}$$

where i,j denote the pixel indices and α and β are the Euler angles defined previously. Now we can evaluate the E & B field from the measured Stokes Q & U parameters by evaluating the following expression,

$$\begin{bmatrix} E_i \\ B_i \end{bmatrix} = -f(\beta_{ij}) \begin{bmatrix} \cos(2\alpha_{ij}) & \sin(2\alpha_{ij}) \\ -\sin(2\alpha_{ij}) & \cos(2\alpha_{ij}) \end{bmatrix} \begin{bmatrix} Q_j \\ U_j \end{bmatrix} , \tag{3.6}$$

where we have used the Einstein summation convention: repeated indices are summed over.

3.2 Evaluating Stokes parameters Q & U fields from E & B fields

To derive the real space operator which translates E & B fields to Stokes parameters Q & U we follow an identical procedure. The inverse relation is as follows,

$$\bar{P} = \bar{T}^{-1} *_2 B * \tilde{T} *_0 B^{\dagger} \bar{S} = \frac{1}{2} \bar{T}^{\dagger} *_2 B * \tilde{T} *_0 B^{\dagger} \bar{S} \tag{3.7}$$

$$= \bar{O}^{-1} * \bar{S} \tag{3.8}$$

It can be shown that the inverse operator is given by the following expression,

$$\bar{O}^{-1} = \begin{bmatrix} -\mathcal{M}_r & \mathcal{M}_i \\ -\mathcal{M}_i & -\mathcal{M}_r \end{bmatrix}_{2N_{\rm pix} \times 2N_{pix}} = -f(\beta_{ij}) \begin{bmatrix} \cos(2\alpha_{ij}) & -\sin(2\alpha_{ij}) \\ \sin(2\alpha_{ij}) & \cos(2\alpha_{ij}) \end{bmatrix} . \tag{3.9}$$

A mere change in the sign on the off-diagonals of the block matrix as compared to Eq. (3.5). We can evaluate the Stokes Q & U parameters from the scalar E & B fields by evaluating the following explicit relation,

$$\begin{bmatrix} Q_i \\ U_i \end{bmatrix} = -f(\beta_{ij}) \begin{bmatrix} \cos(2\alpha_{ij}) & -\sin(2\alpha_{ij}) \\ \sin(2\alpha_{ij}) & \cos(2\alpha_{ij}) \end{bmatrix} \begin{bmatrix} E_j \\ B_j \end{bmatrix} , \tag{3.10}$$

where again the Einstein summation convention is implied.

Here we pause to make a few comments of the different parts of the real space operator. Note that the terms in the square brackets, do not have any multipole ℓ dependence, while the 2α dependence arises from the spin-2 nature of the polarization field. The multipole ℓ dependence is completely built into the radial kernel $f(\beta)$, β being the angular separation between the pixel locations denoted by "i" and "j". The non-locality of the dependence of E & B fields on Stokes Q & U parameters and vice versa, is completely determined by the choice of this radial kernel.

3.3 Decomposing Q & U Stokes parameters into those corresponding to E & B modes respectively

In this section we derive the real space operators which directly decompose the total measured Stokes Q & U parameters to Stokes parameters corresponding to the scalar fields E & B respectively. We follow a procedure similar to that discussed in the previous two sections. Here we need to use the harmonic space E/B projection operators $\tilde{O}_{E/B}$ defined in Eq. (2.10a)

to derive the respective real space operators. It can be shown that the Stokes parameters corresponding to each scalar mode are given by the following expressions,

$$\begin{aligned}\bar{P}_E &= [\bar{T}^{-1} * {}_2B * \tilde{T} * \tilde{O}_E * \tilde{T}^{-1} * {}_2B^\dagger * \bar{T}] * \bar{P}\,, \\ &= [\frac{1}{4}\bar{T}^\dagger * {}_2B * \tilde{T} * \tilde{O}_E * \tilde{T}^\dagger * {}_2B^\dagger * \bar{T}] * \bar{P}\,, \\ &= \bar{O}_E * \bar{P}\,, \end{aligned} \tag{3.11}$$

$$\begin{aligned}\bar{P}_B &= [\bar{T}^{-1} * {}_2B * \tilde{T} * \tilde{O}_B * \tilde{T}^{-1} * {}_2B^\dagger * \bar{T}] * \bar{P}\,, \\ &= [\frac{1}{4}\bar{T}^\dagger * {}_2B * \tilde{T} * \tilde{O}_B * \tilde{T}^\dagger * {}_2B^\dagger * \bar{T}] * \bar{P}\,, \\ &= \bar{O}_B * \bar{P}\,. \end{aligned} \tag{3.12}$$

We contract over all the matrix operators to arrive at the the real space operators. On simplification it can be shows that the real space operator takes up the following form,

$$\bar{O}_{E/B} = 0.5 \begin{bmatrix} \mathcal{I}_r \pm \mathcal{D}_r & -\mathcal{I}_i \pm \mathcal{D}_i \\ -\mathcal{I}_i \pm \mathcal{D}_i & \mathcal{I}_r \mp \mathcal{D}_r \end{bmatrix}_{2N_{\rm pix}\times 2N_{pix}}\,, \tag{3.13}$$

where $\mathcal{I}_r, \mathcal{D}_r, \mathcal{I}_i$ & $\mathcal{D}_i$ are the real and complex parts respectively of the following complex functions,

$$\begin{aligned}\mathcal{I} &= \mathcal{I}_r + i\mathcal{I}_i = \sum_{\ell m} {}_2Y_{\ell m}(\hat{n}_i) {}_2Y^*_{\ell m}(\hat{n}_j)\,, \\ \mathcal{D} &= \mathcal{D}_r + i\mathcal{D}_i = \sum_{\ell m} {}_2Y_{\ell m}(\hat{n}_i) {}_{-2}Y^*_{\ell m}(\hat{n}_j)\,. \end{aligned}$$

These functions can be further simplified using the properties of spin spherical harmonics listed in Appendix 6.1. Specifically it can be shown that these functions reduce to the following mathematical forms,

$$\mathcal{I}(\hat{n}_i, \hat{n}_j) = \sum_\ell \sqrt{\frac{2\ell+1}{4\pi}} {}_2Y_{\ell -2}(\beta_{ij}, \alpha_{ij})\ \mathrm{e}^{-\mathrm{i}2\gamma} = \mathcal{I}_\mathrm{r} + \mathrm{i}\mathcal{I}_\mathrm{i}\,, \tag{3.14a}$$

$$\mathcal{I}_r + i\mathcal{I}_i = \Big[\cos(2\alpha_{ij} + 2\gamma_{ij}) - i\sin(2\alpha_{ij} + 2\gamma_{ij})\Big]_{-2} f(\beta_{ij})\,. \tag{3.14b}$$

$$\mathcal{D}(\hat{n}_i, \hat{n}_j) = \sum_\ell \sqrt{\frac{2\ell+1}{4\pi}} {}_2Y_{\ell +2}\ \mathrm{e}^{-\mathrm{i}2\gamma} = \mathcal{D}_\mathrm{r} + \mathrm{i}\mathcal{D}_\mathrm{i}\,, \tag{3.15a}$$

$$\mathcal{D}_r + i\mathcal{D}_i = \Big[\cos(2\alpha_{ij} - 2\gamma_{ij}) + i\sin(2\alpha_{ij} - 2\gamma_{ij})\Big]_{+2} f(\beta_{ij})\,, \tag{3.15b}$$

where the functions ${}_{\pm2}f_\ell(\beta) = \sum_\ell \sqrt{\frac{2\ell+1}{4\pi}} {}_{\pm2}f_\ell(\beta)$ are completely specified in terms of P^2_ℓ Legendre polynomials and are given by the following explicit mathematical forms,

$$\begin{aligned}{}_{\pm2}f_\ell(\beta) = 2\frac{(\ell-2)!}{(\ell+2)!}\sqrt{\frac{2\ell+1}{4\pi}}\Bigg[&- P^2_\ell(\cos\beta)\left(\frac{\ell-4}{\sin^2\beta} + \frac{1}{2}\ell(\ell-1) \pm \frac{2(\ell-1)\cos\beta}{\sin^2\beta}\right) \\ &+ P^2_{\ell-1}(\cos\beta)\left((\ell+2)\frac{\cos\beta}{\sin^2\beta} \pm \frac{2(\ell+2)}{\sin^2\beta}\right)\Bigg]\,. \end{aligned} \tag{3.16}$$

4 Visualizing the real space operators and quantifying the non-locality of E & B modes

We begin by compare the functions $f, {}_{+2}f$ & ${}_{-2}f$, which we refer to as the radial kernels, since they determine the amplitude of the convolution kernels as a function of the angular distance β from the central pixel. These functions have been calculated by evaluating the multipole sums in Eq. (3.4b) and Eq. (3.16) up to $\ell_{\rm max} = 96$. These resultant functions are depicted in Fig. 1. Note that the function $f(\beta)$, which is a part of the real space convolution kernel which translates the coordinate dependent Stokes Q & U to coordinate independent scalars E & B, has a vanishing contribution from the location where the scalar are being evaluated. This nature of the radial kernel is to be expected in order for it to satisfy the requirement of the scalars being coordinate independent, since any contribution from the local Stokes parameters will necessarily depend on the coordinate definition. The functions ${}_{+2}f(\beta)$ & ${}_{-2}f(\beta)$, both contribute to the convolution kernels which decompose the Stokes parameters into those corresponding to the respective scalar modes E & B. Note that while ${}_{-2}f(\beta)$ specifically contributes at the location of the central pixel, ${}_{+2}f(\beta)$ specifically contributes away from the neighbouring regions.

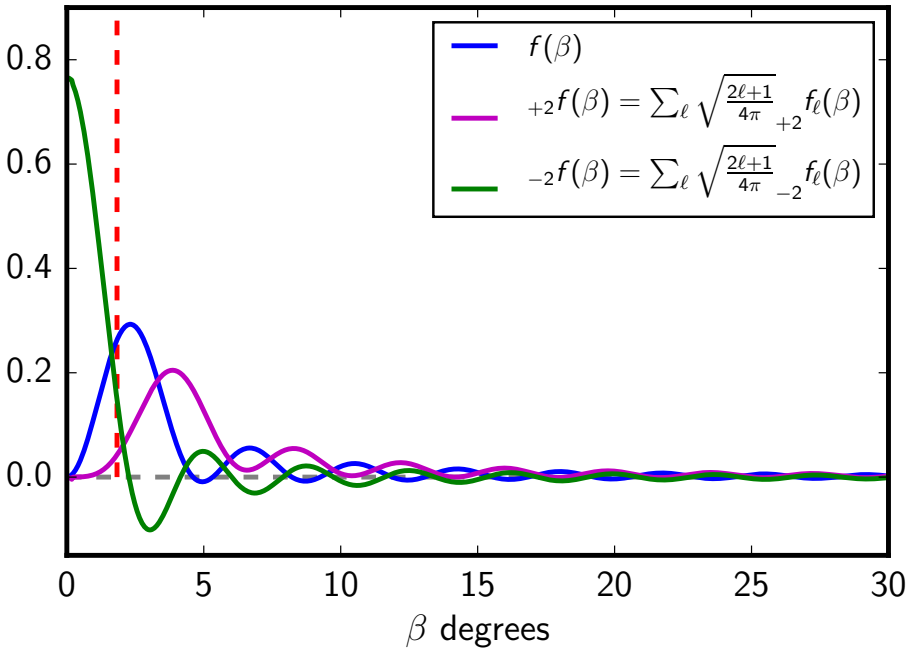

Figure 1. The figure depicts the radial part of the convolution kernels shown in Fig. 2. These radial function have been evaluated with the band limit fixed at $\ell_{\rm max} = 96$. The vertical dashed line marks the approximate size of a NSIDE=32 Healpix pixel.

In addition to the angular distance β from the central pixel, the convolution kernels also depend on the other Euler angles α & γ as seen from Eq. (3.5), Eq. (3.14a) and Eq. (3.15a). We plot the real and imaginary parts of the functions $\mathcal{M}, \mathcal{D}$ & $\mathcal{I}$ at different positions on the sphere. For illustration, these kernel have been evaluated with a band limit of $\ell_{\rm max} = 96$ and sampled using the Healpix pixelization scheme at a very high resolution parameter of NSIDE=2048. The resultant convolution kernels have been evaluated at different locations on the sphere and are depicted in Fig. 2. The function $\mathcal{M}$ is nearly identical irrespective

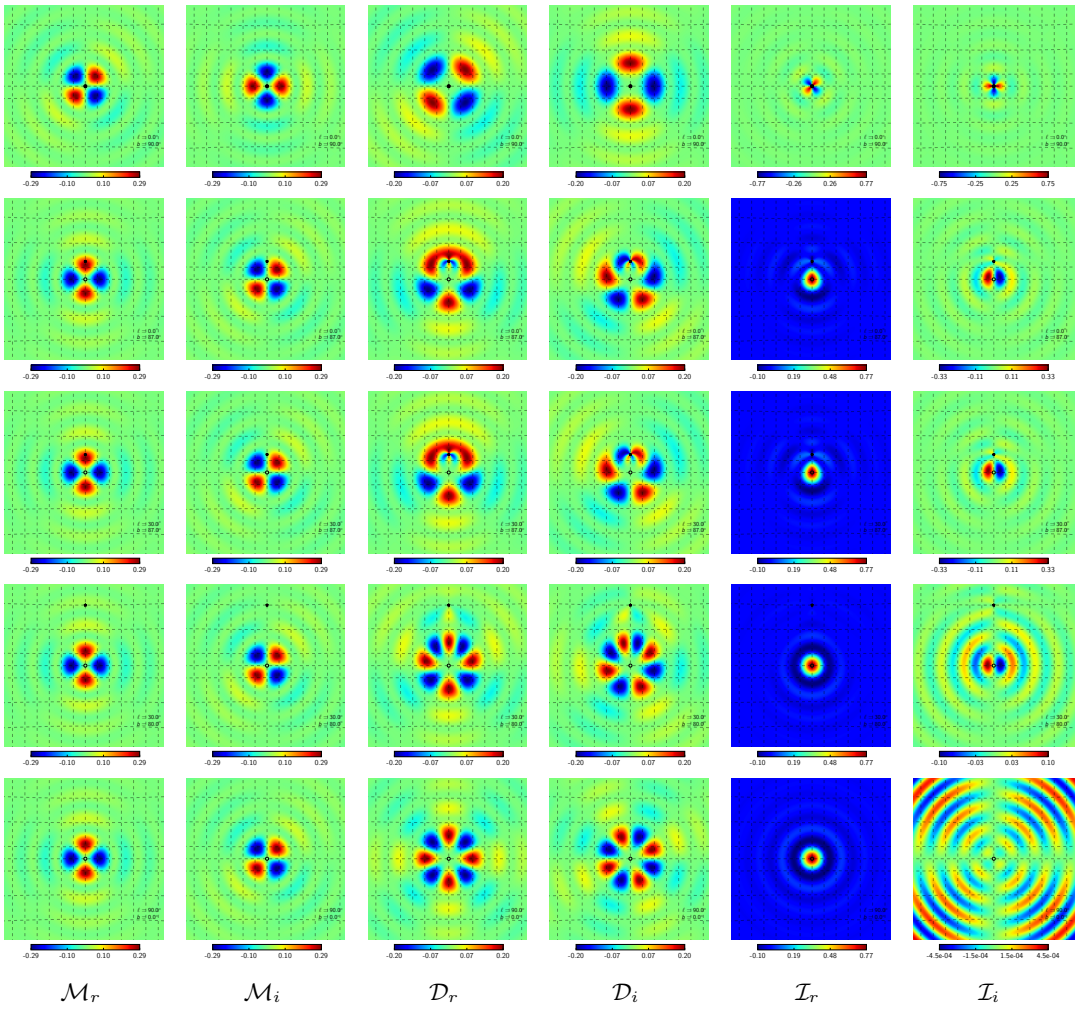

Figure 2. This panel of figure depicts the various parts of the convolution kernel, discussed in Sec. 3. These kernels have been evaluated with the band limit fixed at $\ell_{\rm max} = 96$, however the functions have been sampled at an NSIDE=2048 resolution for visual appeal. The size of each panel is approximately $26^\circ \times 26^\circ$. The black circles denotes the position of the central pixel around which the convolution kernels have been evaluated and the black star marks the location of the north galactic pole. The five rows depict the kernels at different location on the sphere and the galactic coordinates of the central pixel from top to bottom rows are as follows $[b, \ell] = [0^\circ, 0^\circ], [87^\circ, 0^\circ], [87^\circ, 30^\circ], [80^\circ, 30^\circ], [0^\circ, 90^\circ]$.

of changes in the galactic latitude and longitude of the central pixel. The only contrasting locations are the poles (i.e. $|b| = 90^\circ$), where the functions $\mathcal{M}_r$ & $\mathcal{M}_i$ are rotated by 45° as compared to the respective functions evaluated at locations where $|b| \neq 90^\circ$. It is also important to note that these functions are not altered when a part of the domain overlaps with the poles as can be seen in the first four rows of Fig. 2. On the contrary, the function $\mathcal{D}$ varies significantly as a function of galactic latitude of the central pixel. It varies from having a two fold symmetry at the poles to having a four fold symmetry at the equator as seen in the middle two columns of Fig. 2. This transformation likely arises from the distortions induced in this function as parts of its domain passes the galactic poles. The function $\mathcal{I}$ shows similar behavior, varying with latitude, being invariant on changes in the longitude of

the central pixel and being distorted in parts that pass via the galactic pole. This function, in the ideal case of no band limit reduces to a delta function at the position of the central pixel ($\mathcal{I}_r \to \delta(\hat{n}_0 - \hat{n}')$, $\mathcal{I}_i \to 0$), hints of which can be seen by comparing the amplitudes of the real and imaginary parts of this function in the last two columns of Fig. 2. Since we always work with band limited data, both these functions make finite non-zero contributions across the domain. All the function are seen to be invariant under changes in longitude of the central pixel, the latitude being held fixed as can be seen by comparing the figures in the second (evaluated at $[b, \ell] = [87°, 0°]$) and third row (evaluated at $[b, \ell] = [87°, 30°]$) of Fig. 2, as one may have expected.

It is clear that the non-locality of the E and B modes is determined by the radial part of the convolution kernels. To quantify this non-locality as a function of the band limit, we evaluate the radial part of the kernel for different values of the maximum multipole. The resultant functions are plotted in Fig. 3. We define the value of the abscissa at which the function $f_{\mathrm{lmax}}(\beta)$ falls persistently below 1% of the maxima of the function as the non-locality parameter: β_{max}.

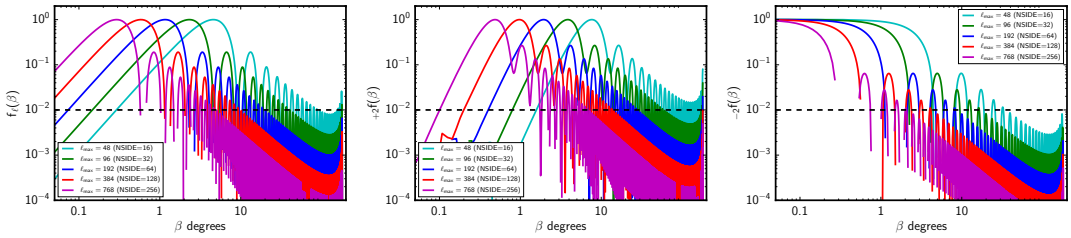

Figure 3. This figure shows a plot of the radial kernels f, f^{+2} & f^{-2} for different band limits as indicated by the legends. The curves for each of these functions have been normalized such that the maximum of the curve is set to unity. The dashed black line marks where the contribution from the curve falls below 1% of the maximum. The dashed vertical lines mark the approximate Healpix pixel sizes at the respective resolution parameter NSIDE.

4.1 Numerical implementation

5 Discussion

6 Appendix

6.1 Mathematical properties of spin spherical harmonics

The spin spherical harmonic functions satisfy the following properties,

$$\sum_{\ell m} {}_sY_{\ell m}(\hat{n}_i) {}_sY^*_{\ell m}(\hat{n}_j) \approx \delta(\hat{n}_i - \hat{n}_j)\,, \tag{6.1a}$$

$$\int {}_sY_{\ell m}(\hat{n}) {}_sY^*_{\ell' m'}(\hat{n}) d\Omega = \delta_{\ell\ell'}\delta_{\rm mm'} \tag{6.1b}$$

Note that the numerical validity of Eq. (**??**) is strictly true only when the sums over the indices (ℓ, m) run to infinity, which is never true in practice since measurements are always band limited. The numerical validity of Eq. (**??**) is only limited by the rate of sampling of these function on the sphere and hence this identity can always be assumed to be strictly valid.

The sum over m index of product of two spherical harmonic functions of spin s_1 and s_2 respectively, is given by the following expression,

$$\sum_m {}_{s_1}Y^*_{\ell m}(\hat{n}_i) {}_{s_2}Y_{\ell m}(\hat{n}_j) = \sqrt{\frac{2\ell+1}{4\pi}} {}_{s_2}Y_\ell^{-s_1}(\beta,\alpha) e^{-is_2\gamma}\,, \tag{6.2}$$

where α, β & γ correspond to the Euler angles that specify the rotation matrix which transforms the local cartesian coordinates defined at $\hat{n}_i$ such that it aligns with the local cartesian coordinate system at $\hat{n}_j$.

While working with CMB polarization one is often dealing with spin-2 spherical harmonics. Here we derive some relation which we use while evaluating the real space projection operators,

$$\sum_{\ell m} {}_2Y_{\ell m}(\hat{n}_i) {}_2Y^*_{\ell m}(\hat{n}_j) = \tag{6.3}$$

6.2 Function forms of radial kernels

$$\begin{aligned} f_\ell^{+2}(\cos\beta) = 2\frac{(\ell-2)!}{(\ell+2)!}\sqrt{\frac{2\ell+1}{4\pi}}\Bigg[&- P_\ell^2(\cos\beta)\left(\frac{\ell-4}{\sin^2\beta} + \frac{1}{2}\ell(\ell-1) + \frac{2(\ell-1)\cos\beta}{\sin^2\beta}\right) \\ &+ P^2_{\ell-1}(\cos\beta)\left((\ell+2)\frac{\cos\beta}{\sin^2\beta} + \frac{2(\ell+2)}{\sin^2\beta}\right)\Bigg] \end{aligned} \tag{6.4a}$$

$$\begin{aligned} f_\ell^{-2}(\cos\beta) = 2\frac{(\ell-2)!}{(\ell+2)!}\sqrt{\frac{2\ell+1}{4\pi}}\Bigg[&- P_\ell^2(\cos\beta)\left(\frac{\ell-4}{\sin^2\beta} + \frac{1}{2}\ell(\ell-1) - \frac{2(\ell-1)\cos\beta}{\sin^2\beta}\right) \\ &+ P^2_{\ell-1}(\cos\beta)\left((\ell+2)\frac{\cos\beta}{\sin^2\beta} - \frac{2(\ell+2)}{\sin^2\beta}\right)\Bigg] \end{aligned} \tag{6.4b}$$